

# MASSIVE AND NEWLY DEAD: DISCOVERY OF A SIGNIFICANT POPULATION OF GALAXIES WITH HIGH VELOCITY DISPERSIONS AND STRONG BALMER LINES AT $Z \sim 1.5$ FROM DEEP KECK SPECTRA AND HST/WFC3 IMAGING

RACHEL BEZANSON<sup>1</sup>, PIETER VAN DOKKUM<sup>1</sup>, JESSE VAN DE SANDE<sup>2</sup>, MARIJN FRANX<sup>2</sup>, MARISKA KRIEK<sup>3</sup>

*Submitted to ApJ Letters*

## ABSTRACT

We present deep Keck/LRIS spectroscopy and HST/WFC3 imaging in the rest-frame optical for a sample of eight galaxies at  $z \sim 1.5$  with high photometrically-determined stellar masses. The data are combined with VLT/XShooter spectra of five galaxies from van de Sande et al. (2011, 2012 to be submitted). We find that these thirteen galaxies have high velocity dispersions, with a median of  $\sigma = 301 \text{ km s}^{-1}$ . This high value is consistent with their relatively high stellar masses and compact sizes. We study their stellar populations using the strength of Balmer absorption lines, which are not sensitive to dust absorption. We find a large range in Balmer absorption strength, with many galaxies showing very strong lines indicating young ages. The median  $H\delta_A$  equivalent width, determined directly or inferred from the H10 line, is  $5.4 \text{ \AA}$ , indicating a luminosity-weighted age of  $\sim 1 \text{ Gyr}$ . Although this value may be biased towards higher values because of selection effects, high-dispersion galaxies with such young ages are extremely rare in the local Universe. Interestingly we do not find a simple correlation with rest-frame  $U - V$  color: some of the reddest galaxies have very strong Balmer absorption lines. These results demonstrate that many high-dispersion galaxies at  $z \sim 1.5$  were quenched recently. This implies that there must be a population of star-forming progenitors at  $z \sim 2$  with high velocity dispersions or linewidths, which are notoriously absent from CO/H $\alpha$  selected surveys.

## 1. INTRODUCTION

In the local universe, massive galaxies are primarily ellipticals with little ongoing star-formation and red colors. Recent surveys have identified plausible progenitors of these galaxies at redshifts  $z = 1 - 2$ , finding that they have small sizes for their mass (e.g. Daddi et al. 2005; Trujillo et al. 2006; Toft et al. 2007; Zirm et al. 2007; van Dokkum et al. 2008). Furthermore, by using rest-frame colors to isolate the bluest dead galaxies (e.g. Kriek et al. 2010; Whitaker et al. 2012), it appears that a significant fraction of them have young ages. These blue galaxies may be similar to the well-known “E+A” galaxies found among low mass galaxies at lower redshift (e.g. Dressler & Gunn 1983; Couch & Sharples 1987; Zabludoff et al. 1996), although Whitaker et al. (2012) note that the label “A galaxies” may be more appropriate at high redshift as they may lack an underlying old component.

These results are quite exciting and suggest that at  $z \sim 1 - 2$  we are beginning to see the build-up of the massive end of the red sequence. However, this conclusion is based on two main assumptions. First, the inclusion of these young galaxies in samples of massive galaxies depends on estimates of stellar mass. Such estimates suffer from systematic uncertainties such as the IMF and the contribution of thermally pulsating asymptotic giant branch (TPAGB) stars (e.g. Maraston 2005; Kriek et al. 2010; Zibetti et al. 2012). Second,

especially at  $z \gtrsim 1.5$ , the identification of galaxies as young and old, star-forming vs. quiescent is again based on the SED shapes, more specifically on the shape of the Balmer/4000  $\text{\AA}$  break, which depends sensitively on proper treatment of dust reddening and thus is uncertain. Up to now, very few direct measurements of the ages (e.g. Kriek et al. 2009) and masses (e.g. Cappellari et al. 2009; van Dokkum et al. 2009; Newman et al. 2010; Onodera et al. 2010; Martinez-Manso et al. 2011; van de Sande et al. 2011; Toft et al. 2012) of massive galaxies exist at  $z > 1$ .

With spectroscopic data, one can circumvent these uncertainties. Balmer absorption lines, which are prominent in the spectra of A stars and will only be present in a galaxy spectrum for  $\sim 1 \text{ Gyr}$  after star formation has ceased, can be used as luminosity-weighted age indicators. As an example, Le Borgne et al. (2006) identified recently quenched  $H\delta$ -strong (HDS) galaxies at  $z \sim 1.2$  in the Gemini Deep Deep Survey. These measurements are particularly valuable when combined with velocity dispersions, which provide a direct measurement of the depth of the potential well and can be combined with structural parameters to calculate dynamical (rather than photometric) masses.

In this study, we present a sample of eight massive galaxies with deep Keck I spectroscopy using the LRIS instrument (and five with X-Shooter spectra from van de Sande et al. (2011, 2012 to be submitted)) in combination with rest-frame optical imaging from WFC3 and ACS on HST. Using this exceptional dataset, we are able to confirm that all of the galaxies in the sample have high velocity dispersions (and high dynamical masses). From this unique sample, we conclude that there is a significant population of recently quenched galaxies with

<sup>1</sup> Department of Astronomy, Yale University, New Haven, CT 06520-8101

<sup>2</sup> Sterrewacht Leiden, Leiden University, NL-2300 RA Leiden, Netherlands

<sup>3</sup> Department of Astronomy, University of California, Berkeley, CA 94720, USA

very high velocity dispersions at  $z \sim 1.5$ .

## 2. DATA

### 2.1. High- $z$ Surveys & Target Selection

For this project, a sample of massive, bright galaxies was selected from the Newfirm Medium Band Survey (NMBS) and UKIDSS UDS fields. The NMBS catalogs include photometry in the COSMOS and AEGIS fields in a multitude of deep broadband and medium band optical and near-IR wavebands and includes medium band photometry in the near-IR to sample the Balmer/4000 Å break in galaxies at these redshifts (Whitaker et al. 2011). The UDS field (Williams et al. 2009) also provides deep optical and near-IR photometry over a large  $0.77 \text{ deg}^2$  field. For both survey catalogs, we use the EAzY software (Brammer et al. 2008) to calculate photometric redshifts and InterRest (Taylor et al. 2009) to calculate rest-frame colors for all galaxies in the fields. We use FAST (Kriek et al. 2009) to estimate stellar masses, assuming Bruzual & Charlot (2003) (BC03) stellar population models and a Chabrier (2003) Initial Mass Function (IMF). Primary targets were selected to have  $I < 24.0$  and  $\log M_* \gtrsim 11$ .

In Fig. 1, the properties of massive galaxies included in our three masks are shown as colored points along with galaxies with  $\log M_* > 11$  and  $1.2 < z < 1.6$  in the NMBS COSMOS field. Following Williams et al. (2009) we discriminate between star-forming (blue points) and young/old quiescent (red points) galaxies using rest-frame  $U - V$  and  $V - J$  colors. Our sample spans a large range in  $I$ -band magnitudes and rest-frame  $U - V$  colors. However, as is usually the case with spectroscopic samples, our sample is somewhat biased toward bright magnitudes and blue colors. This may imply that we are biased towards the inclusion of newly quenched galaxies, since the bluest, youngest galaxies will also be the brightest galaxies in the sample and therefore will have the highest S/N for a given exposure time. Furthermore, although we do not select explicitly for compactness, galaxies that have more concentrated light will also have higher S/N ratios. Because of this we may also have a bias toward smaller galaxies at fixed mass (see van de Sande et al, in preparation).

### 2.2. Velocity Dispersions and Balmer Line Strengths

Spectroscopic data were collected using LRIS on the Keck I telescope during two four-night runs in January and April, 2010. Observations were performed with the upgraded red arm using the  $600 \text{ mm}^{-1}$  grating. All observations consist of sequences of three dithered 15 minute exposures, offset by  $3''$  each. We observed galaxies in four different slit masks, two in the COSMOS field (18 hours, 6.75 hours), one in the AEGIS field (15 hours) and one in the UDS field (10.5 hours). Reduction of the spectra was performed in IRAF following standard techniques, as described in van Dokkum & Stanford (2003). No fringe correction was necessary due to the reduced interference fringing in the LBNL detectors (Rockosi et al. 2010).

We measure velocity dispersions using *PPXF* (Cappellari & Emsellem 2004), allowing the program to fit individual BC03 single stellar population (SSP) models with 8th-order additive and 3rd-order

multiplicative polynomials. Best-fit broadened templates (red) are plotted with galaxy spectra in Fig. 2. We estimate the measurement errors on the dispersion measurements by shuffling the residuals from the fits, adding them back to the template and allowing *PPXF* to refit the dispersion. We only include galaxies for which the measurement error is less than 10% of the measured velocity dispersion in the following analysis. We verify that velocity dispersion measurements are not strongly dependent on the choice of polynomials and are stable within the quoted error bars. Velocity dispersions are aperture corrected to  $r_e/8$  using the size measurements described in the following subsection and the prescription  $\sigma_0 = \sigma_{ap}(8.0r_{ap}/r_e)^{0.066}$ , based on the dynamical modeling of the SAURON sample (Cappellari et al. 2006).

Traditionally,  $H\delta_A$  has been used as a galaxy age indicator (e.g. Kauffmann et al. 2003). However due to the redshifts of these galaxies and spectral coverage of LRIS, it is only available for the lowest redshift galaxies in this sample. Instead, we measure H10; defining bandpasses to measure a pseudocontinuum ( $[3780.0 - 3785.0 \text{ \AA}]$  and  $[3810.0 - 3815.0 \text{ \AA}]$ ) and line ( $[3783.0 - 3813.0 \text{ \AA}]$ ) from all spectra, convolved to  $300 \text{ km s}^{-1}$ . Template fluxes from the dynamical modeling are substituted for masked pixels and errors are estimated using 1000 bootstrap iterations with shuffled residuals. We convert from H10 to Lick  $H\delta_A$  as follows. Using BC03 templates, also convolved to  $\sigma = 300 \text{ km s}^{-1}$ , we measure both H10 and  $H\delta_A$  and find a tight correlation for templates older than  $\sim 100 \text{ Myr}$ . We fit the relation with a polynomial and calculate inferred  $H\delta_A$  as:

$$H\delta_A = -16.37 + 10.45H10 - 1.44H10^2 + 0.08H10^3. \quad (1)$$

We also measure  $3727 \text{ \AA}$  OII emission using the bandpasses defined by Fisher et al. (1998) and estimate errors as described above.

### 2.3. Structural Parameters

Sizes of all galaxies in our sample are measured from Hubble Space Telescope (HST) imaging. For seven of the galaxies, we use F160W imaging from the WFC3 camera, sampling the rest-frame  $R$  band. Observations were conducted with a four point dither pattern, offset by half pixel increments. We interlace the flat-fielded frames to increase the resolution of the galaxy images and better sample the point-spread function (PSF), without introducing smoothing inherent in drizzling. We use a similarly interlaced TinyTim PSF, initially oversampled by a factor of 10, shifted to reflect the dither pattern, interlaced in the same manner and finally binned to the resolution of the interlaced galaxy images. We extract postage stamps from the interlaced frames centered on each galaxy, aggressively mask other objects using SExtractor (Bertin & Arnouts 1996) segmentation maps and use Galfit (Peng et al. 2002) to fit Sérsic profiles to the galaxy images. We verify that these measurements are quite consistent (with a scatter of 3%) with those made from the drizzled images produced by the HST pipeline and a nearby PSF star.

For the single galaxy for which WFC3 imaging is not available we measure its size from ACS imaging and dis-

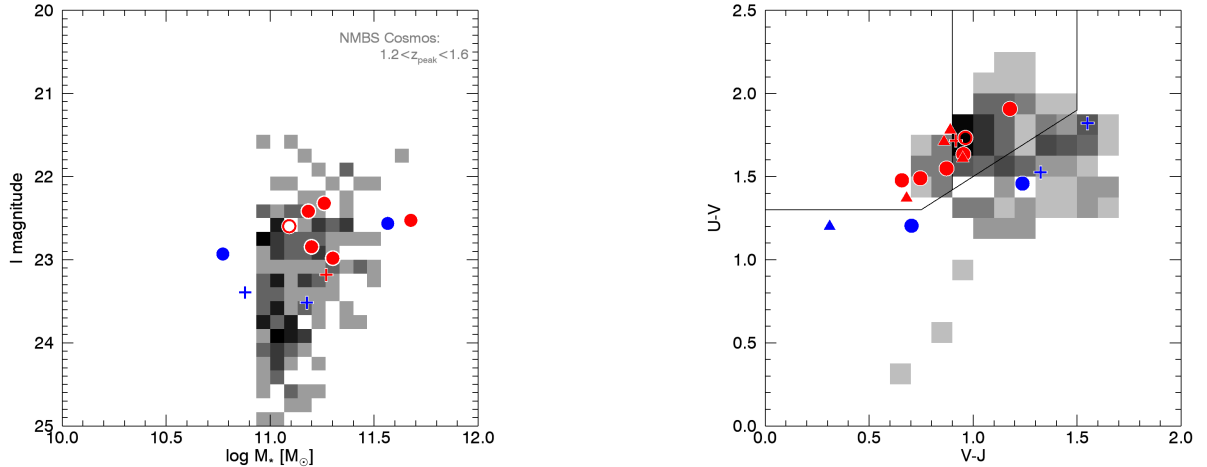


FIG. 1.— Properties of the massive  $z \sim 1.5$  spectroscopic galaxy sample (colored symbols, crosses indicate insufficient spectroscopic S/N) and overall population of massive  $1.2 < z < 1.6$  galaxies in the NMBS COSMOS field (gray). (a) I magnitude vs. stellar mass sample selection. (b) rest-frame U-V vs. V-J colors with black outlines highlighting the phase space location of young and old quiescent galaxies as defined in Whitaker et al. (2011). Six galaxies in the sample are red and dead, while two galaxies have ongoing star-formation; their red color can be attributed to dust. Triangles indicate van de Sande (2011, 2012 to be submitted) sample.

tinguish this data point as an open circle in Figures 3 and 4. We use ACS imaging from the COSMOS team, cutting a postage stamp from the v.1.3 ACS F814W mosaic from Scoville et al. (2007) and using an isolated PSF star. We note that although the F814W is bluestward of rest-frame optical for this galaxy, it is at the lowest redshift of the sample and the bandpass effects should be minimal.

### 3. THE EXTREME DYNAMICS AND STELLAR POPULATIONS OF $Z \sim 1.5$ MASSIVE GALAXIES

#### 3.1. High Velocity Dispersions and Masses

As can be seen in Table 1, the galaxies have very high velocity dispersions; the median  $\sigma_0$  for the complete sample is  $301 \text{ km s}^{-1}$ . In the local Universe, such high dispersions are rare, and typical of giant galaxies at the centers of groups or clusters such as NGC 4374, NGC 4472, and M87. This is demonstrated in the left panel of Fig. 3, where we show our sample with colored points and data from the SDSS in grey. The  $z \sim 1.5$  galaxies fall on the high dispersion tail of the SDSS distribution.

The high dispersions are fully consistent with the high stellar masses and small sizes of the galaxies. This is shown explicitly in Fig. 3a, as we compare the measured velocity dispersions to the velocity dispersion inferred from the size, Sérsic index, and stellar mass, scaling by the average factor between stellar mass and structural-corrected  $M_{\text{dyn}}$  in the SDSS (Franx et al. 2008; Taylor et al. 2009; van de Sande et al. 2011; Bezanson et al. 2011, 2012). We calculate  $\sigma_{\text{inf}}$  as:

$$\sigma_{\text{inf}} = \sqrt{\frac{GM_{\star}}{0.557K_V(n)r_e}}, \quad (2)$$

with

$$K_V(n) = \frac{73.32}{10.465 + (n - 0.94)^2} + 0.954, \quad (3)$$

as derived by Bertin et al. (2002). This constant corresponds to velocity dispersions within  $r_e/8$ .

There is good agreement between inferred and measured velocity dispersions, although there may be a small systematic offset. This may be caused by the fact that galaxies with extremely high velocity dispersions are rare, locally and  $z \sim 1.5$  (e.g. Bezanson et al. 2011). Based on the steep high dispersion tail of the velocity dispersion function (VDF), galaxies with high  $\sigma_{\text{inf}}$  are more likely to be scattered above the  $\sigma_{\text{inf}} - \sigma_0$  relation than to have intrinsically high  $\sigma_0$ . Therefore for a sample of galaxies drawn from this distribution, the relation will veer from one-to-one at high dispersions. We simulate this effect by selecting samples of galaxies uniformly in  $\sigma_{\text{inf}}$  from the local  $\Phi(\sigma_0)$  (Bernardi et al. 2010) plus 0.06 dex scatter between  $\sigma_0$  and  $\sigma_{\text{inf}}$ . We include a polynomial fit to the resulting relation (red line) in Fig. 3a. Inferred dispersion remains a good predictor of measured velocity dispersion for this sample, although the data suggest that the scatter may be higher at  $z \sim 1.5$  (Bezanson et al. 2011).

For completeness, we directly compare stellar and dynamical masses in Fig. 3b. Dynamical masses were calculated for each galaxy from its size, velocity dispersion and best-fit Sérsic index (e.g. Bertin et al. 2002; Cappellari et al. 2006; Taylor et al. 2010):

$$M_{\text{dyn}} = \frac{K_V(n)\sigma^2 r_e}{G}. \quad (4)$$

The most massive galaxies in the sample lie directly on top of the local relation, while the lower mass galaxies lie closer to the one-to-one line. There is a hint that overall stellar masses are closer to dynamical masses at higher redshifts, increasing the ratio from a median of  $\log(M_{\star}/M_{\text{dyn}}) = 0.27$  dex locally to 0.09 dex at  $z \sim 1.5$ . However, the local stellar-to-dynamical mass relation exhibits a fair amount of scatter, and due to the biased nature of this sample of galaxies it is hard to disentangle whether this offset is due to evolution and/or selection

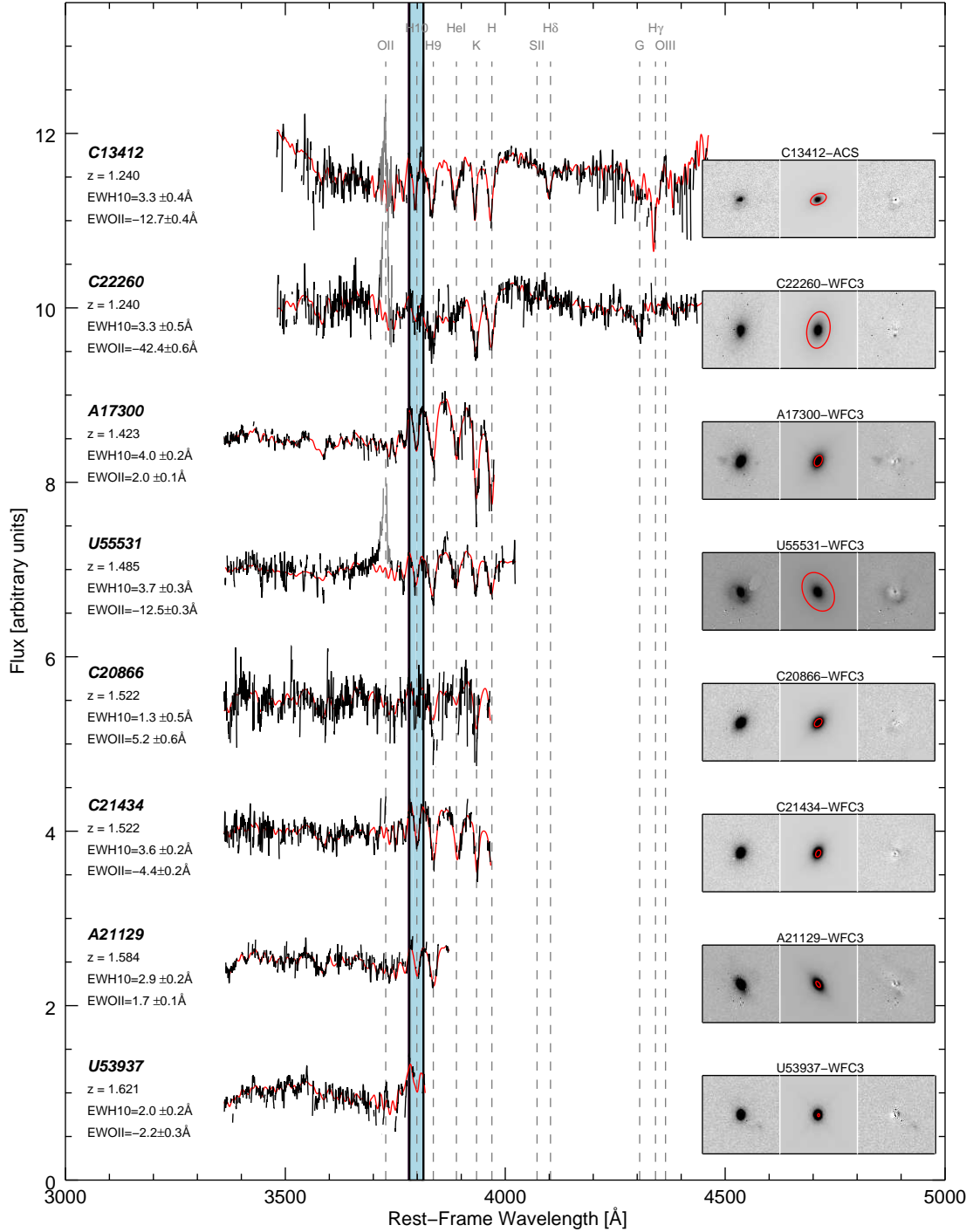


FIG. 2.— LRIS spectra with best-fit BC03 templates (red) and HST imaging for  $z \sim 1.5$  massive galaxy sample. H10 bandpass labeled with blue band. OII emission lines (grey), when present, are masked in dispersion fitting. Imaging Panels: *left*: Image, *center*: Best-fit Sérsic model with  $r_e$  ellipse (red) *right*: residual image.

TABLE 1  
 MEASUREMENTS FOR  $z \sim 1.5$  MASSIVE GALAXY SAMPLE WITH LRIS SPECTROSCOPY.

ID	$z_{\text{spec}}$	$r_{e,c}$ [kpc]	n	b/a	$M_{\star}$ [ $M_{\odot}$ ]	$\sigma_{\text{inf}}$ [ $\text{km s}^{-1}$ ]	$\sigma_{\text{meas}}$ [ $\text{km s}^{-1}$ ]	$\sigma_0$ [ $\text{km s}^{-1}$ ]	$M_{\text{dyn}}$ [ $M_{\odot}$ ]	H10 [Å]	OII [Å]
A17300	1.4235	2.9	5.3	0.64	$11.26 \pm 0.1$	375	$265 \pm 7$	$312 \pm 8$	$11.36 \pm 0.05$	$4.0 \pm 0.2$	$2.0 \pm 0.1$
A21129	1.5839	1.5	5.0	0.50	$11.18 \pm 0.1$	459	$260 \pm 9$	$319 \pm 12$	$11.12 \pm 0.05$	$2.9 \pm 0.2$	$1.7 \pm 0.1$
C13412 <sup>a</sup>	1.2395	4.2	6.0	0.62	$11.09 \pm 0.1$	274	$116 \pm 8$	$133 \pm 9$	$10.72 \pm 0.06$	$3.3 \pm 0.3$	$-12.7 \pm 0.4$
C22260	1.2399	9.3	4.1	0.63	$11.68 \pm 0.1$	292	$249 \pm 16$	$271 \pm 17$	$11.86 \pm 0.06$	$3.3 \pm 0.5$	$-42.4 \pm 0.7$
C21434	1.5223	1.9	3.1	0.65	$11.20 \pm 0.1$	337	$218 \pm 16$	$264 \pm 20$	$11.24 \pm 0.06$	$3.6 \pm 0.2$	$-4.4 \pm 0.3$
C20866	1.5222	2.4	3.0	0.67	$11.30 \pm 0.1$	329	$272 \pm 23$	$324 \pm 27$	$11.54 \pm 0.07$	$1.3 \pm 0.6$	$5.2 \pm 0.6$
U53937	1.6210	0.8	3.6	0.75	$10.77 \pm 0.1$	335	$231 \pm 19$	$296 \pm 24$	$10.92 \pm 0.07$	$2.0 \pm 0.2$	$-2.2 \pm 0.3$
U55531	1.4848	11.2	4.9	0.72	$11.57 \pm 0.1$	261	$257 \pm 24$	$277 \pm 26$	$11.87 \pm 0.07$	$3.7 \pm 0.3$	$-12.5 \pm 0.3$

<sup>a</sup>Morphology measured from ACS imaging

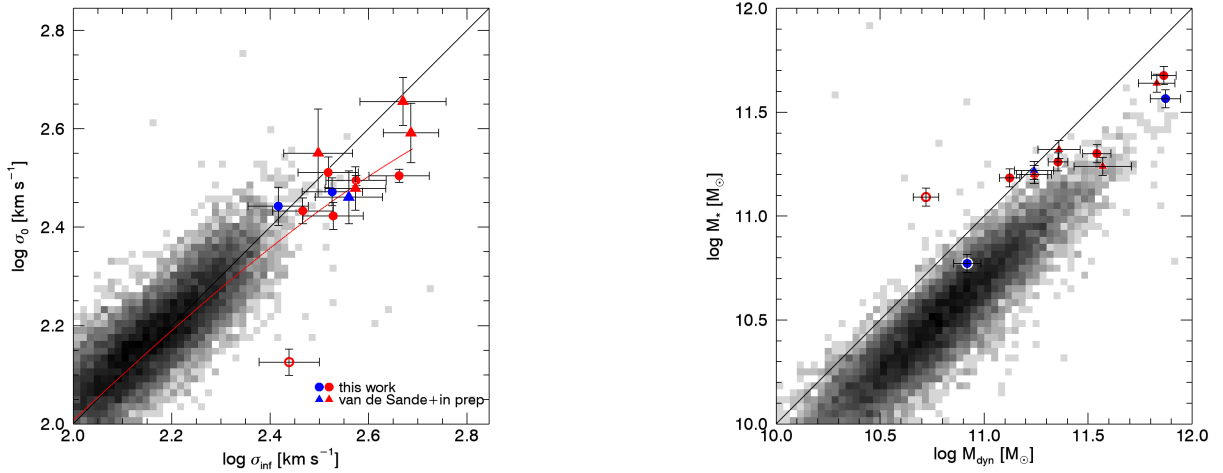


FIG. 3.— (a) Inferred versus measured velocity dispersions for  $z \sim 1.5$  sample (colored points) and massive galaxy sample in the SDSS (greyscale). LRIS sample are circles (WFC3-filled, ACS-open) and X-Shooter sample (van de Sande, in prep) are triangles. As in Fig. 1, color-coding is based on rest-frame color derived quiescence. The high redshift galaxies have very high dispersions, coinciding with the tail of the SDSS distribution. Inferred dispersion appears to be a reasonable predictor of intrinsic velocity dispersion, even at the highest dispersions. (b) Dynamical versus stellar mass for high and low redshift galaxies.

effects. In all cases, we verify that the galaxies in this sample are dynamically massive.

### 3.2. Using Balmer Line Strengths to Identify Recently Quenched Galaxies

We find that the galaxies exhibit a large range in Balmer line strengths, with H10 ranging from  $1.3 - 4.0 \text{ \AA}$  ( $H\delta_A = -4.8 - 7.6 \text{ \AA}$ ). The immediate implication is that they have a large range in ages and/or a recent burst contribution. Furthermore, the median Balmer line strength is quite high at H10 =  $3.3 \text{ \AA}$  ( $H\delta_A = 5.4 \text{ \AA}$ ). This is a remarkable result given the high dispersions of the galaxies. Fig. 4a shows the relation between Balmer line strength and velocity dispersion for SDSS galaxies (grey) and our data (colored). The Balmer lines at  $z \sim 1.5$  are dramatically stronger, and show a much larger range, than at  $z = 0$ . This is arguably the most direct evidence yet for rapid quenching of massive galaxies at  $z \sim 1.5$ , as the quantities on both axes are directly measured and completely independent from photometric data. We note that Le Borgne et al. (2006) also showed a strongly increasing fraction of galaxies with strong Balmer lines out to  $z \sim 1.2$ , although their sample had lower photometric masses ( $\log M > 10.2$ ) and lacked velocity dispersion measurements.

In Fig. 4b we interpret the Balmer lines in the context of the stellar population synthesis (SPS) models of Bruzual & Charlot (2003). The distribution of Balmer line strengths is indicated in the bottom panel and can be interpreted in terms of ages using the top panel. The observed range in line strengths implies luminosity-weighted ages ranging from several hundred Myrs to maximally old stellar populations, with a median of  $\sim 1 \text{ Gyr}$ .

An obvious question is whether we could have drawn the same conclusions from photometric data. Fig. 4c compares the Balmer line strengths and rest-frame  $U - V$  colors for the galaxies in this sample and to SPS models. The models are BC03 single population tracks for three different metallicities (grey) and double-burst models (green and orange dot-dashed) in which 10% and 1% of the galaxy’s mass is formed in a secondary burst 4 Gyr after the original episode of star-formation. Although the *range* in colors of this sample of galaxies implies a similar range in ages as the Balmer lines do, the data do not follow the model predictions. Specifically, the data show no anti-correlation between color and Balmer line strength, as would be expected. Some of the bluest galaxies have weak Balmer lines, and some of the reddest have strong Balmer lines.

A possible explanation is that the colors are affected by dust reddening, and Fig. 4c illustrates the importance of independent measures of age. To compare the intrinsic distribution of colors/ages, one could design “dust-corrected” colors (e.g. Brammer et al. 2009), however these depend strongly on SED modeling and well-determined dust estimates. We also note that the sample of 13 is barely adequate for this particular test; larger, unbiased samples may show the expected correlation between Balmer lines and colors, as strongly suggested by

the complete samples of Whitaker et al. (2012).

## 4. DISCUSSION AND CONCLUSIONS

We have identified a population of galaxies at  $z \sim 1.5$  with high velocity dispersions and strong Balmer absorption lines. These results confirm that by  $z \sim 1.5$  the population of massive galaxies is much less uniform than it is locally: instead of being red, dead ellipticals, many have experienced recent star-formation within  $\sim 1 \text{ Gyr}$  (see also Le Borgne et al. 2006; van Dokkum & Brammer 2010; van Dokkum et al. 2011; Whitaker et al. 2012). A direct implication is that  $\lesssim 1 \text{ Gyr}$  earlier, at  $z \sim 2$ , there must exist highly star-forming progenitor galaxies with similarly high velocity dispersions. Such galaxies have yet to be identified, and the fact that some of the youngest galaxies in our sample are also the reddest suggests that these progenitors may have a very high dust content.

The results are also consistent with our study of the velocity dispersion function of quiescent and star forming galaxies (Bezanson et al. 2012), as we concluded that quenching must occur efficiently for galaxies with high velocity dispersions. This conclusion was based on the rapid build-up of the VDF of quenched galaxies and the stability of the star-forming VDF since  $z \sim 1.5$ . The discovery of this population of young, high-dispersion galaxies is strong evidence in favor of this model.

In addition to having different stellar populations at  $z \gtrsim 1.5$ , a flurry of studies in the last decade have uncovered the dramatic size evolution that massive galaxies have undergone in the last 10 billion years (e.g. Daddi et al. 2005; Trujillo et al. 2006; Toft et al. 2007; Zirm et al. 2007; van Dokkum et al. 2008). The temporal correlation between the structural evolution and recently quenched stars presents a tempting connection between the events which halt star-formation in massive galaxies and at the same time cause them to be compact relative to their local analogs. Whitaker et al. (2012) found there to be no correlation between color of quiescent galaxies and their sizes, however it would be interesting to investigate the size evolution based on a larger, more representative sample of spectroscopic data to estimate galaxy ages.

We note that the selection and observational biases may influence the distribution of galaxies in this sample. In this context our study is complimentary to Whitaker et al. (2012), which is mass complete for galaxies in the NMBS but relies solely on SEDs to estimate photometric redshifts, stellar masses and rest-frame colors to derive galaxy ages. However, we note that while qualitatively the results are similar, we find a puzzling lack of (anti-)correlation between color and Balmer line strength: neither the star-forming galaxies nor the bluest quiescent galaxies in our sample necessarily have the strongest Balmer lines.

As is often the case, larger samples are needed to explore these issues. With increasingly powerful multiplexed spectroscopic instruments and excellent space-based imaging we can construct large samples of galaxies at this pivotal epoch and simultaneously study the structural properties and stellar populations of all types of dynamically massive galaxies.

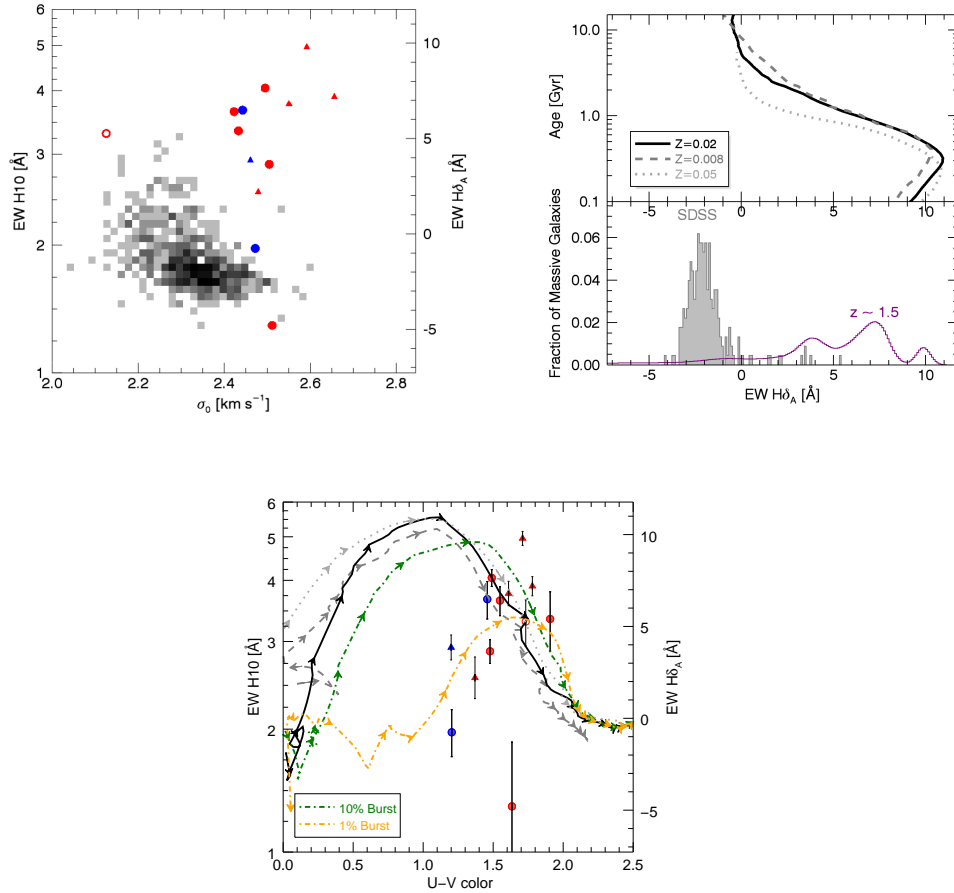


FIG. 4.— (a) Balmer EWs versus velocity dispersion for massive galaxies. The majority of galaxies in this sample have the highest velocity dispersions known at any redshift. Unlike the uniformly old, dead stellar populations in comparable galaxies at  $z \sim 0$ , many of these galaxies have strong Balmer lines, implying recent quenching. (b) Top: Age versus  $\text{H}\delta_A$  for BC03 SSP templates of varied metallicity. Bottom:  $\text{H}\delta_A$  distribution from high-dispersion ( $\log \sigma > 2.4$ ) galaxies in the SDSS (grey) and  $z \sim 1.5$  distribution (purple) with individual galaxies included as gaussians of width equal to their measurement errors. In striking contrast with local high-dispersion galaxies, which have uniformly weak Balmer lines and old luminosity-weighted ages, this sample exhibits a broad distribution of EWs including many with strong Balmer lines and young ages. (c) Balmer EWs versus rest-frame U-V colors relative to BC03 SSP (grey) and double-burst (green and orange) models. Even though the colors and Balmer lines suggest a similar range in ages for the galaxies in this sample, the galaxies do not follow the simple model tracks which suggests the importance of dust or secondary bursts of star formation in these systems.

## REFERENCES

- Bernardi, M., Shankar, F., Hyde, J. B., Mei, S., Marulli, F., & Sheth, R. K. 2010, *MNRAS*, 404, 2087
- Bertin, E., & Arnouts, S. 1996, *A&AS*, 117, 393
- Bertin, G., Ciotti, L., & Del Principe, M. 2002, *A&A*, 386, 149
- Bezanson, R., van Dokkum, P., & Franx, M. 2012, *ArXiv e-prints*
- Bezanson, R., et al. 2011, *ApJ*, 737, L31+
- Brammer, G. B., van Dokkum, P. G., & Coppi, P. 2008, *ApJ*, 686, 1503
- Brammer, G. B., et al. 2009, *ApJ*, 706, L173
- Bruzual, G., & Charlot, S. 2003, *MNRAS*, 344, 1000
- Cappellari, M., & Emsellem, E. 2004, *PASP*, 116, 138
- Cappellari, M., et al. 2006, *MNRAS*, 366, 1126
- . 2009, *ApJ*, 704, L34
- Chabrier, G. 2003, *PASP*, 115, 763
- Couch, W. J., & Sharples, R. M. 1987, *MNRAS*, 229, 423
- Daddi, E., et al. 2005, *ApJ*, 626, 680
- Dressler, A., & Gunn, J. E. 1983, *ApJ*, 270, 7
- Fisher, D., Fabricant, D., Franx, M., & van Dokkum, P. 1998, *ApJ*, 498, 195
- Franx, M., van Dokkum, P. G., Schreiber, N. M. F., Wuyts, S., Labbé, I., & Toft, S. 2008, *ApJ*, 688, 770
- Kauffmann, G., et al. 2003, *MNRAS*, 341, 33
- Kriek, M., van Dokkum, P. G., Labbé, I., Franx, M., Illingworth, G. D., Marchesini, D., & Quadri, R. F. 2009, *ApJ*, 700, 221
- Kriek, M., et al. 2010, *ApJ*, 722, L64
- Le Borgne, D., et al. 2006, *ApJ*, 642, 48
- Maraston, C. 2005, *MNRAS*, 362, 799
- Martinez-Manso, J., et al. 2011, *ApJ*, 738, L22
- Newman, A. B., Ellis, R. S., Treu, T., & Bundy, K. 2010, *ApJ*, 717, L103
- Onodera, M., et al. 2010, *ApJ*, 715, L6
- Peng, C. Y., Ho, L. C., Impey, C. D., & Rix, H.-W. 2002, *AJ*, 124, 266
- Rockosi, C., et al. 2010, in *Society of Photo-Optical Instrumentation Engineers (SPIE) Conference Series*, Vol. 7735, Society of Photo-Optical Instrumentation Engineers (SPIE) Conference Series
- Scoville, N., et al. 2007, *ApJS*, 172, 1
- Taylor, E. N., Franx, M., Brinchmann, J., van der Wel, A., & van Dokkum, P. G. 2010, *ApJ*, 722, 1
- Taylor, E. N., et al. 2009, *ApJS*, 183, 295
- Toft, S., Gallazzi, A., Zirm, A., Wold, M., Zibetti, S., Grillo, C., & Man, A. 2012, *ApJ*, 754, 3
- Toft, S., et al. 2007, *ApJ*, 671, 285
- Trujillo, I., et al. 2006, *ApJ*, 650, 18
- van de Sande, J., et al. 2011, *ApJ*, 736, L9
- van Dokkum, P. G., & Brammer, G. 2010, *ApJ*, 718, L73

- van Dokkum, P. G., Kriek, M., & Franx, M. 2009, *Nature*, 460, 717
- van Dokkum, P. G., & Stanford, S. A. 2003, *ApJ*, 585, 78
- van Dokkum, P. G., et al. 2008, *ApJ*, 677, L5
- . 2011, *ApJ*, 743, L15
- Whitaker, K. E., Kriek, M., van Dokkum, P. G., Bezanson, R., Brammer, G., Franx, M., & Labbé, I. 2012, *ApJ*, 745, 179
- Whitaker, K. E., et al. 2011, *ApJ*, 735, 86
- Williams, R. J., Quadri, R. F., Franx, M., van Dokkum, P., & Labbé, I. 2009, *ApJ*, 691, 1879
- Zabludoff, A. I., Zaritsky, D., Lin, H., Tucker, D., Hashimoto, Y., Sheckman, S. A., Oemler, A., & Kirshner, R. P. 1996, *ApJ*, 466, 104
- Zibetti, S., Gallazzi, A., Charlot, S., Pierini, D., & Pasquali, A. 2012, *ArXiv e-prints*
- Zirm, A. W., et al. 2007, *ApJ*, 656, 66